Medical Engineering & Physics 26 (2004) 165–175

Medical Engineering & Physics

www.elsevier.com/locate/medengphy

A structural fingertip model for simulating of the biomechanics of tactile sensation

J.Z. Wu [*,a], R.G. Dong [a], S. Rakheja [b], A.W. Schopper [a], W.P. Smutz [a]

[a] National Institute for Occupational Safety and Health, Morgantown, WV 26505, USA
[b] Concordia University, Montreal, Quebec H3G 1M8, Canada

Received 7 January 2003; received in revised form 14 August 2003; accepted 30 September 2003

Abstract

Tactile performance of human fingertips is associated with activity of the nerve endings and sensitivity of the soft tissue within the fingertip to the static and dynamic skin indentation. The nerve endings in the fingertips sense the stress/strain states developed within the soft tissue, which are affected by the material properties of the tissues. The vibrotactile sensation and tactile performance are thus believed to be strongly influenced by the nonlinear and time-dependent properties of the soft tissues. The purpose of the present research is to simulate the biomechanics of tactile sensation. A two-dimensional model, which incorporates the essential anatomical structures of a finger (i.e. skin, subcutaneous tissue, bone, and nail), has been used for the analysis. The skin tissue is assumed to be hyperelastic and viscoelastic. The subcutaneous tissue is considered to be a nonlinear, biphasic material composed of a hyperelastic solid and an inviscid fluid phase. The nail and bone are considered to be linearly elastic. The advantages of the proposed fingertip model over the previous "waterbed" and "continuum" fingertip models include its ability to predict the deflection profile of the fingertip surface, the stress and strain distributions within the soft tissue, and most importantly, the dynamic response of the fingertip to mechanical stimuli. The proposed model is applied to simulate the mechanical responses of a fingertip under a line load, and in one-point (1PT) and two-point (2PT) tactile discrimination tests. The model's predictions of the deflection profiles of a fingertip surface under a line load agree well with the reported experimental data. Assuming that the mechanoreceptors in the dermis sense the stimuli associated with normal strains (the vertical and horizontal strains) and strain energy density, our numerical results suggest that the threshold of 2PT discrimination may lie between 2.0 and 3.0 mm, which is consistent with the published experimental data. The present study represents an effort to develop a structural model of the fingertip that incorporates its anatomical structure, and the nonlinear and time-dependent properties of the soft tissues.
Published by Elsevier Ltd on behalf of IPEM.

Keywords: Hyperelastic; Poroelastic; Finite element model; Soft tissue mechanics; Tactile sensation

1. Introduction

The tactile senses, in general, include the sensation of touch, pressure, vibration, and temperature. Humans primarily use their fingertips in the exploration of the external world through the sense of touch. When the fingertips come in contact with an object, the tactile receptors beneath the skin respond to deformation of the skin by transmitting electrical impulses to the brain through the peripheral nerve system [1]. The primary features of the transmitted signals, the frequencies of nerve impulses, are associated with the mechanical environment of the tactile receptors, e.g. stress and strain [2]. The presence of multiple mechanoreceptors that respond to mechanical stimuli in different ways has been reported by Verrillo and Gescheider [3]. The study of fingertip biomechanics is vital to enhance an understanding of the mechanism of tactile sensation and sensory thresholds.

The human fingertip is complex from a mechanical and structural point of view. Macroscopically, a fingertip is composed of skin layers (epidermis and dermis),

* Corresponding author. Tel.: +1-304-285-5832; fax: +1-304-285-6265.
E-mail address: jwu@cdc.gov (J.Z. Wu).

1350-4533/$ - see front matter Published by Elsevier Ltd on behalf of IPEM.
doi:10.1016/j.medengphy.2003.09.004

subcutaneous tissue, arterial bone, and nail. The epidermis, the outermost layer of the skin, consists of primarily protective horny structures, such as stratum corneum. The dermis, a fibrous layer supporting the epidermis, contains numerous mechanoreceptors [4] which have been classified into four types [5]. The subcutaneous tissue is a fat layer which primarily consists of lipocytes. The matrix of the subcutaneous tissue contains approximately 60–72% fluid in volume [6]. The biomechanical properties of the skin and the subcutaneous tissues influence the transmission of mechanical stimuli (i.e. stress and strain) through the tissues, and thus, play an important role in the tactile sensation.

In order to avoid the difficulties associated with complex mechanical behavior and structures of the skin and subcutaneous tissues, two types of simplified models of fingertips have been proposed in the literature: "waterbed" and "continuum" models. In the "waterbed" models [7,8], a fingertip is represented by an incompressible fluid representing the subcutaneous tissue enclosed by an elastic or hyperelastic membrane representing the skin. Although the "waterbed" models have been applied to predict the deflection of fingertip surface under a static, line load [7] and the static force-deflection characteristics [8], they cannot predict the mechanical stimuli which the mechanoreceptors receive at different locations within the skin. This is attributed to their inability to analyze variations in the stress and strain within the tissues due to the considerations of uniform tension in the membrane and uniform fluid pressure. Phillips and Johnson [9] and Srinivasan and Dandekar [10] proposed "continuum" fingertip models where the skin and subcutaneous tissues were represented by homogeneous, isotropic, and incompressible elastic media. The continuum fingertip models predict the stress and strain distributions within the tissues, and thus the response profiles of the receptors within the skin tissue. However, the force-deformation response and the deflection profile of the skin surface predicted by these two models did not agree with experimental observations [10]. All these published fingertip models are two-dimensional (2D). To our knowledge, there is no published three-dimensional (3D) fingertip model. Generally, absolute values of force response cannot be predicted using a 2D model. However, the trends of the variations in force response as a function of time and the contact conditions can be predicted reasonably using a 2D model [11]. Compared to a detailed 3D model, the 2D model has the advantage of providing cost-effective solutions for parametric studies, especially for complex nonlinear problems.

The soft subcutaneous and skin tissues are known to exhibit nonlinear and time-dependent material properties [12–14], and, consequently, the response of fingertips to mechanical loading is expected to be nonlinear and time-dependent. Zhang et al. [15] suggested that the mechanical behavior of the skin and the subcutaneous tissue can be simulated using the nonlinear biphasic constitutive model [16]. Since the tactile sensation is known to depend on the nature of the mechanical stimuli (frequency and magnitude), contact force and contact area [17], the effects of nonlinearity and time-dependency of the soft tissues are expected to have a substantial influence on vibrotactile sensation and tactile performance, which are related to activity of the nerve endings at the fingertips, and sensitivity of the soft subcutaneous tissue to skin indentation. The reported fingertip models do not incorporate the nonlinear and time-dependent effects associated with the anatomical substructures and tissue material properties. The purpose of the present research was to simulate the mechanics of tactile sensation of a fingertip using a multi-layered fingertip model. A two-dimensional model is proposed that incorporates the essential anatomical structures of a finger: skin, subcutaneous tissue, bone, and nail. The skin tissue is assumed to be hyperelastic and viscoelastic. The subcutaneous tissue is considered to be a nonlinear, biphasic material composed of a hyperelastic solid and an inviscid fluid phase. The hydraulic permeability of the subcutaneous tissue is considered to be deformation-dependent. The mechanical responses of a fingertip under a line load, and in one-point (1PT) and two-point (2PT) tactile discrimination tests are simulated using the proposed model.

2. Methods

2.1. Finite element model

The biomechanics of tactile sensation of a fingertip are analyzed using a multi-layered 2D finite element (FE) model, as shown in Fig. 1(a). The fingertip is assumed to be composed of a skin layer (representing epidermis and dermis), subcutaneous tissue, bone, and nail. The dimensions of the fingertip are assumed to be representative of the index finger of a male subject [18]. The skin is assumed to have a thickness of 0.8 mm. The cross-sections of the fingertip and the bone are assumed to be elliptical and the tissue thickness is considered to be asymmetric about the bone (Fig. 1(a)): the tissue thickness between the bone and the pulp skin surface is assumed to be greater than that between the bone and the nail. The biquadral, plain-strain elements were used in the finite element models. The commercial finite element software package ABAQUS (Hibbitt, Karlsson, and Sorensen, Inc., Pawtucket, USA; version 6.2) was applied for the analysis.

The skin tissue, including epidermis and dermis, is assumed to be nonlinearly elastic (hyperelastic) and lin-

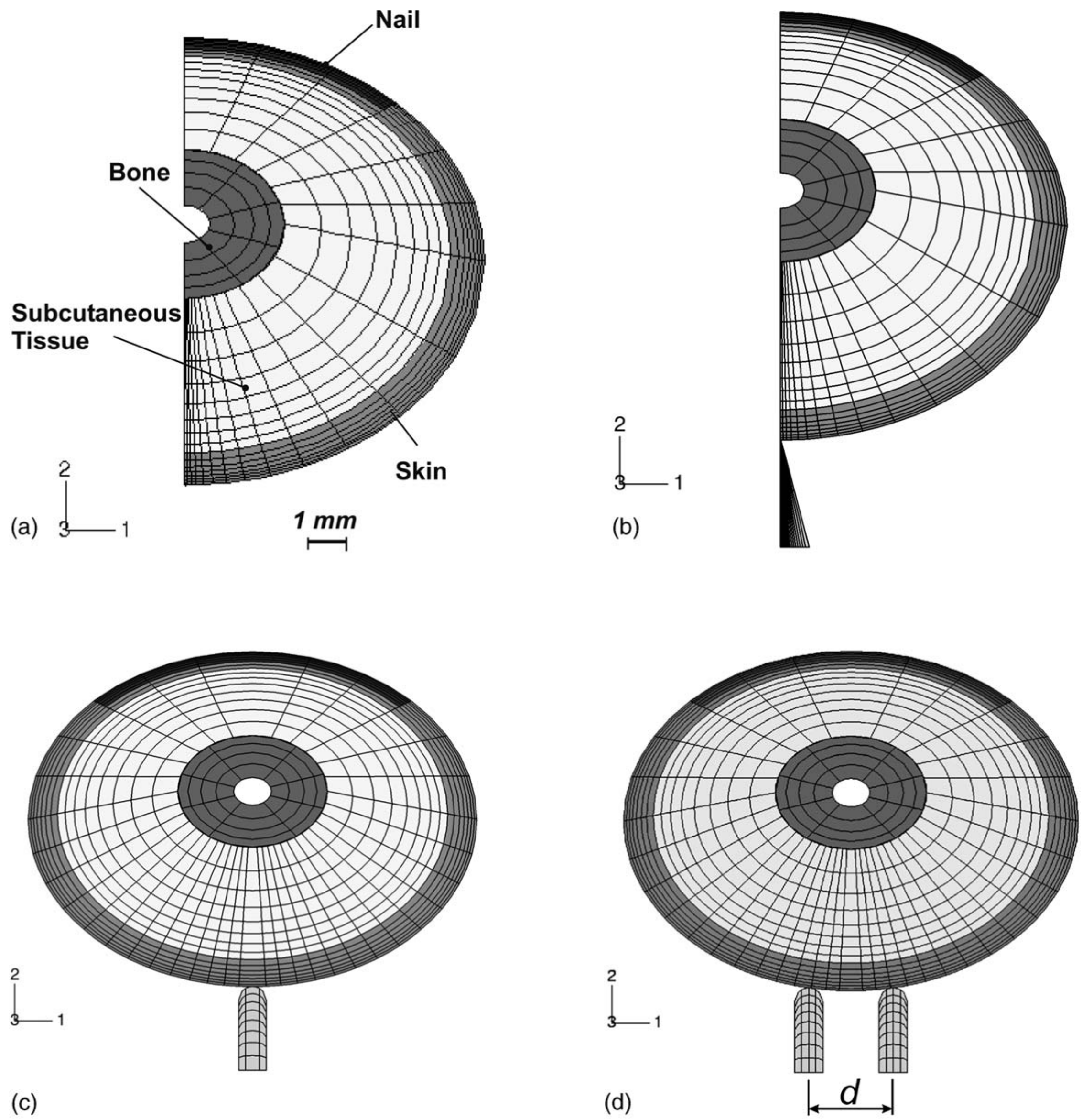

Fig. 1. Finite element modeling of fingertip. (a) The fingertip is composed of skin, subcutaneous tissue, bone, and nail; the skin tissue is assumed to be nonlinearly elastic and linearly viscoelastic, the subcutaneous tissue is assumed to be a biphasic material composed of a fluid phase and a hyperelastic phase, and the bone and nail are considered as linear elastic. (b) Indentation of the fingertip using a sharp wedge. The wedge has widths of 50 μm and 1.2 mm on the tip and base, respectively, and a height of 3.0 mm, and is assumed to be of hard plastic. (c) One-point (1PT) indentation test of the fingertip. (d) Two-point (2PT) indentation test of the fingertip. The indentors have a width of 1 mm and a circular contacting surface, and are assumed to be of steel.

early viscoelastic. The subcutaneous tissue is assumed to be a biphasic material composed of a fluid phase and a hyperelastic solid phase. The nail and the bone are considered to be linearly elastic. The constitutive relations of the skin and subcutaneous tissue are discussed in detail in [11,19], and attached in Appendix A. Detailed information on how the governing equations of hyperelastic and poroelastic materials are solved numerically and how the continuity equations are satisfied in ABAQUS has been described in the ABAQUS Theory Manual [20]. Simon [21] showed that the poroelastic model, as used in ABAQUS, is equivalent to the biphasic model provided that the fluid phase is inviscid. Wu et al. [22] have further evaluated the application of ABAQUS for solving the biomechanical problems and found that the biphasic models for soft tissues can be implemented into ABAQUS.

2.2. Numerical tests

Two series of numerical tests have been performed in this study. The first series of tests were performed to simulate the mechanical responses of a fingertip under a line load, as shown in Fig. 1(b). The fingertip was fixed at the center on the nail surface, while a steel wedge with sharp edge (edge thickness = 50 μm) was moved towards the skin surface in a ramp manner, such that a skin deformation of 1 mm was realized within a ramping period of 1 s. The position of the wedge was then kept constant for 100 s, to allow for relaxation of the reaction force at the fingertip. The reaction force, and the distributions of displacement, fluid pressure, stresses and strains within the soft tissue were computed as a function of time using the FE model. The predicted skin surface deflections of the fingertip were compared with the experimental results reported by Srinivasan [7].

The second series of tests were performed to study the mechanics of tactile sensation of the fingertip in one-point (1PT) and two-point (2PT) discrimination tests. The fingertip was fixed on the center of the nail surface, while either one or two steel bars (each with a circular contact surface and thickness of 1 mm) was used to deform the skin surface of the fingertip by 1 mm within a ramping period of 1 s (Fig. 1(c) and (d)). A total of five numerical tests were performed within this series, where the first test was carried out using one single steel bar (Fig. 1(c)). The remaining four tests were performed using two steel bars with different spacing between the bars (Fig. 1(d)), d= 1.5, 2.0, 3.0, and 4.0 mm, respectively. The analyses were performed to compute the displacement, stress and strain fields within the soft tissue at the state of maximum depression (t= 1 s).

The contact of fingertip/wedge or fingertip/indenter was assumed to be frictionless. The wedge and indenters were assumed to be of steel (linearly elastic). The center of the fingernail surface was fixed in both horizontal and vertical directions, while the wedge or indenter was prescribed to a vertical movement towards the fingertip. No other boundary conditions were assumed in the simulations.

3. Results

Using the proposed fingertip model (Fig. 1(b)), the surface deflection of the fingertip indented by a wedge-shaped probe was determined. The predicted profiles of the skin surface deflection at t= 1 s (when the wedge approaches the maximum displacement of 1 mm) and 100 s were compared with the experimental measurements by Srinivasan [7], as shown in Fig. 2. The skin surface deflection, as predicted by our model, decreased slightly as a function of time, while the position of the wedge was kept unchanged. The skin surface deflection tends to approach a steady-state, as time increases. After approximately 20 s, the variation of the skin surface deflection became negligible (results not shown); therefore, skin surface deflection at 100s (Fig. 2) represents approximately the steady-state profile. The steady-state profile of the skin surface deflection (Fig. 2, t= 100 s) derived from our model agrees well with the experimental data by Srinivasan [7]. Some deviations between the computed and measured data were observed, particularly as the distance from load exceeded 2.5 mm.

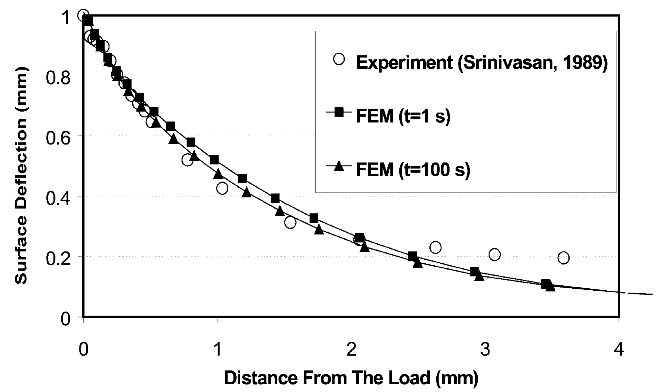

Fig. 2. Comparison of the predicted profile of skin surface deflection with the experimental data reported by Srinivasan [7]. The numerical tests were performed using the configuration shown in Fig. 1(b).

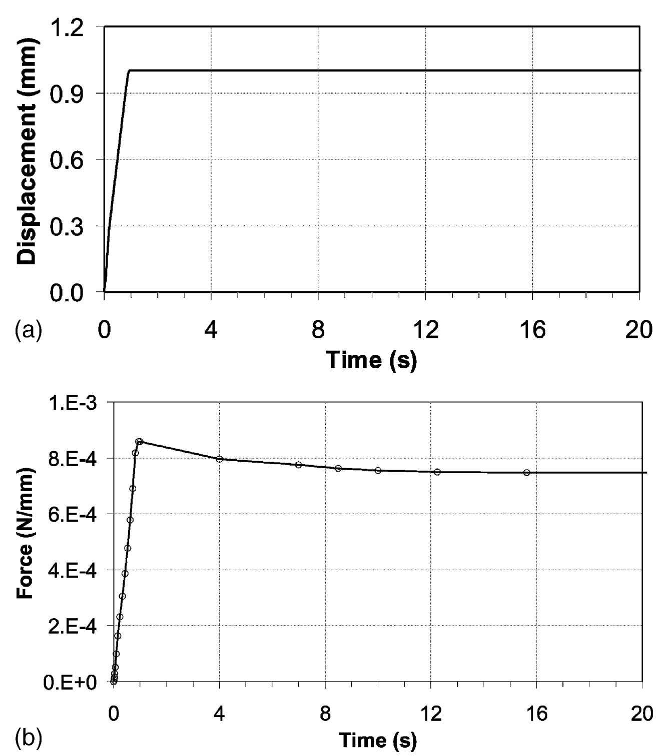

Fig. 3. Model prediction of the loading curves of a fingertip indented using a sharp wedge. (a) Prescribed displacement history of the indenting wedge. (b) Predicted contact force as a function of time. The numerical tests were performed using the configuration shown in Fig. 1(b). In this two-dimensional model, the contact force, F, is expressed as the force in unit length (N/mm).

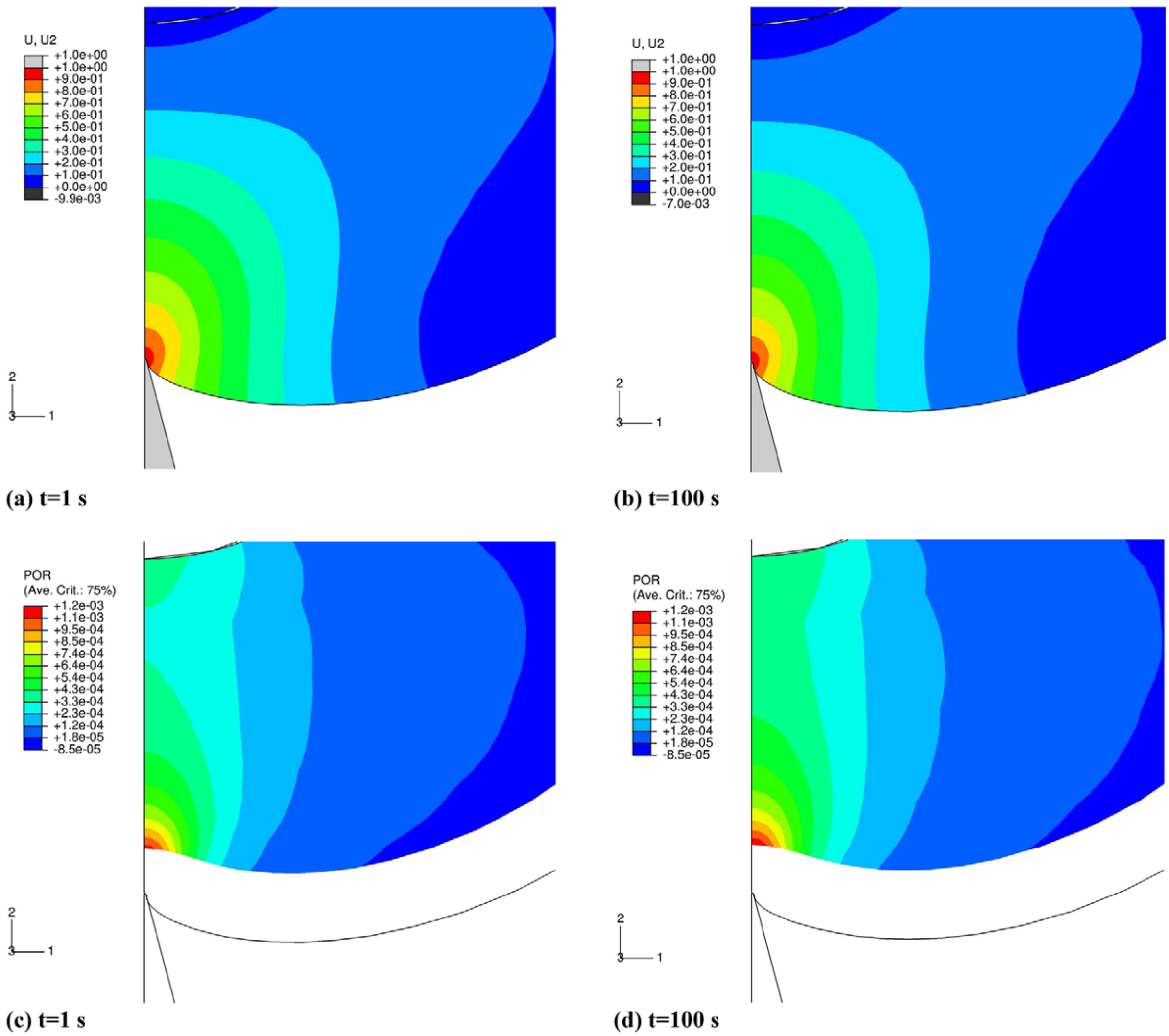

Fig. 4. Predicted distributions of the displacement in the vertical direction and fluid pressure within the fingertip indented using a sharp wedge. (a) Vertical displacement ($U2$) for $t = 1$ s. (b) Vertical displacement ($U2$) for $t = 100$ s. (c) Fluid pressure (POR) for $t = 1$ s. (d) Fluid pressure (POR) for $t = 100$ s. The unit for the displacement is mm and that for the fluid pressure is MPa. The numerical tests were performed using the configuration shown in Fig. 1(b).

Fig. 3 shows the time histories of the prescribed displacement and the resulting reaction force acting on the wedge. In the 2D FE model, the force is measured in intensity, i.e. force per unit length (N/mm). The reaction force is increased in a linear ramp manner in response to the prescribed indentation of the wedge. Although the displacement of the wedge was held constant (1 mm) at $t > 1$ s, the reaction force tended to decrease in time (Fig. 3(b)). Most of the decay in the reaction force occurred within a short period ($1 < t < 20$ s). The variation of the reaction force is negligible at $t > 20$ s.

The fields of the displacement in the loading direction and the fluid pressure within the soft tissue for $t = 1$ s (Fig. 4(a) and (c)) are compared with those for $t = 100$ s (Fig. 4(b) and (d)). A comparison of Fig. 4(a) and (b) suggests almost negligible variations in the surface deflection. The displacement distribution within the tissue, however, varied slightly because of tissue relaxation. The time-dependent response of tissue deformation and reaction force is mainly attributed to the redistribution of the fluid pressure and the fluid flow within the biphasic subcutaneous tissue, as demonstrated in Fig. 4(c) and (d).

The distributions of the maximum and minimum normal strains, shear strain, and strain energy density at depths of 0.50, 0.75, and 1.00 mm from the undeformed skin surface were derived over the width of the fingertip, and are shown in Fig. 5(a)–(d), respectively. The maximum (tensile) strain of the tissue predominantly occurs in a direction parallel to the skin surface, while the minimum (compressive) strain mostly occurs in a direction normal to the skin surface. The maximum and minimum strain and strain energy

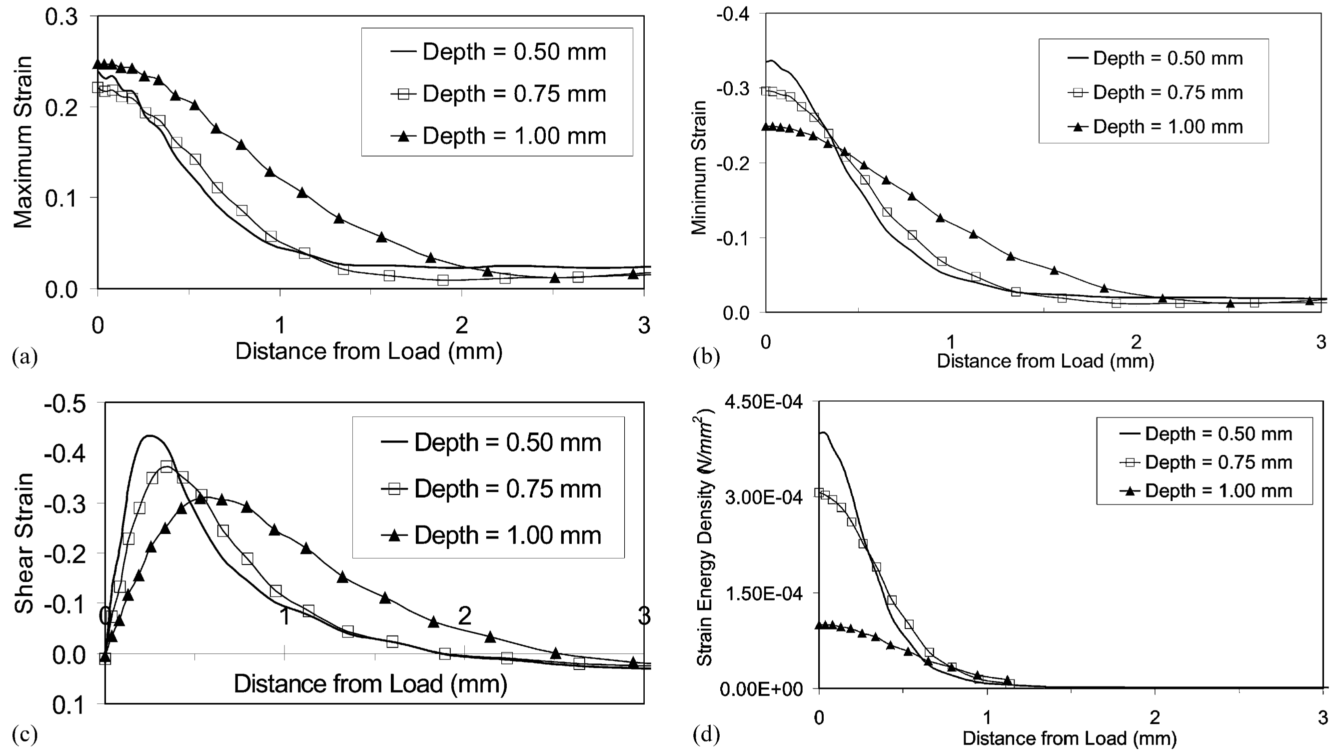

Fig. 5. Predicted distributions of the maximum and minimum strains, shear strain, and strain energy density in the soft tissue of the fingertip indented using a sharp wedge (at depths of 0.50, 0.75, and 1.00 mm within the tissue, and at $t = 1$ s). (a) Maximum strain. (b) Minimum strain. (c) Shear strain. (d) Strain energy density. The strains are defined in logarithm strain. The numerical tests were performed using the configuration shown in Fig. 1(b). The time history of the prescribed displacement of the indentation wedge is shown in Fig. 3(a).

density exhibit their maximal magnitudes in the immediate vicinity of the contact point, while the shear strain reverses its direction around the contact point.

Fig. 6 illustrates the distributions of vertical displacements at a depth of 0.75 mm from the undeformed skin surface for the one-point (1PT) and two-point (2PT) indentations. The figure also illustrates the deflection

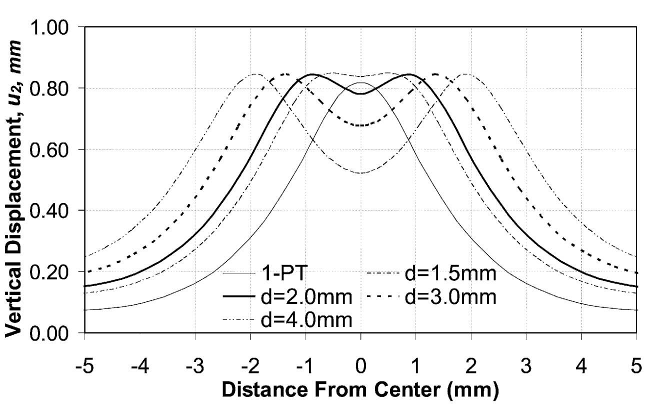

Fig. 6. Predicted distributions of the displacement in the vertical direction (u_2) in the soft tissue of the fingertip (at a depth of 0.75 mm within the tissue) for 1PT and 2PT indentations ($t = 1$ s). The numerical tests were performed using the configurations shown in Fig. 1(c) and (d).

response as a function of indentor spacing, d, in the case of the 2PT indentation test. The peak displacement occurs at the contact points for both the 1PT and 2PT indentations. For the 2PT test, the difference between the displacement at the center and that at the contact points increases with the increasing spacing between the indentors.

The distribution of strains in the horizontal and the vertical direction at a depth of 0.75 mm from the undeformed skin surface for 1PT and 2PT indentations is illustrated in Fig. 7(a) and (b), respectively. The difference between the strain values at the center and those at the contact points decreased with the decreasing spacing between the indentors. It is interesting to note that, when the indentor spacing, d, decreased from 4.0 to 1.5 mm, the positive peak strain values under the contacting point changed very little, while the strain values at the center changed considerably. The variation in the magnitudes of the normal strains at the center of the fingertip is relatively small when the spacing between the indentors was increased from 3.0 to 4.0 mm or reduced from 2.0 to 1.5 mm (Fig. 7). However, a reduction in the indentor spacing from 2.0 to 1.5 mm produced a significant variation in the strain values.

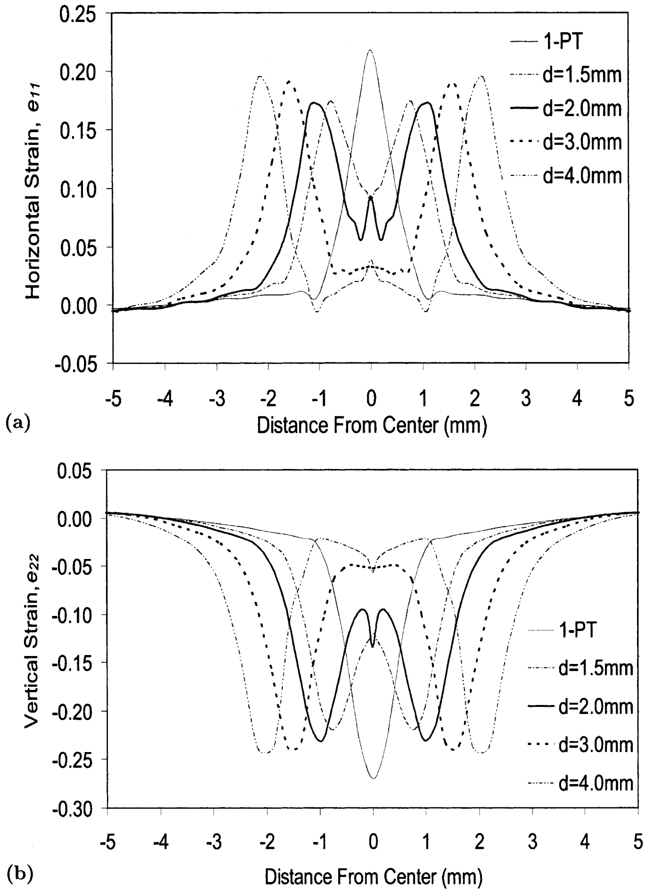

Fig. 7. Predicted distributions of the logarithm strains in the horizontal (e_{11}) and vertical (e_{22}) directions in the soft tissue of the fingertip (at a depth of 0.75 mm within the tissue) for 1PT and 2PT indentations (t= 1 s). (a) Horizontal strain. (b) Vertical strain. The numerical tests were performed using the configurations shown in Fig. 1(c) and (d).

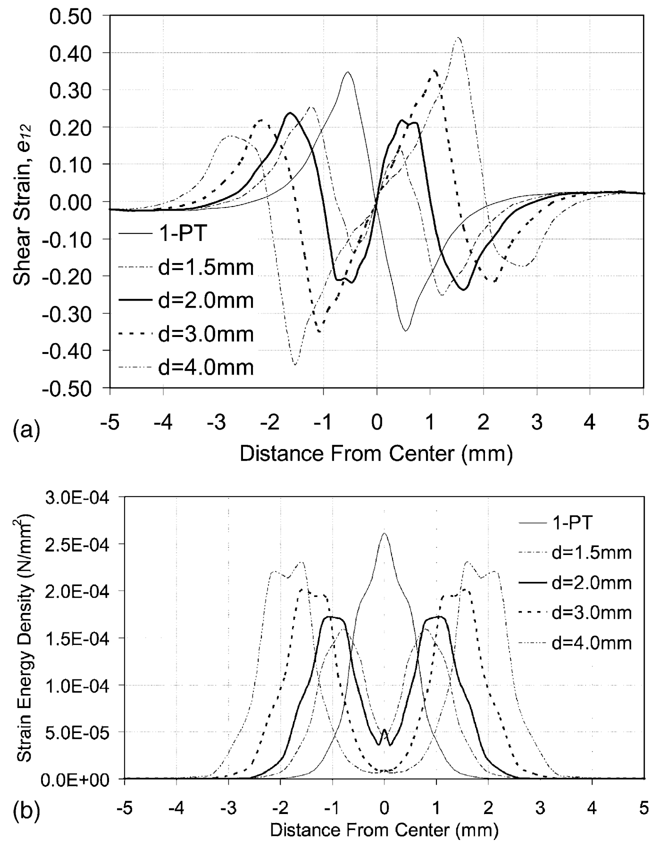

Fig. 8. Predicted distributions of the logarithm shear strains (e_{12}) and strain energy density (SED) in the soft tissue of the fingertip (at a depth of 0.75 mm) for 1PT and 2PT indentations (t= 1 s). (a) Shear strain. (b) Strain energy density. The numerical tests were performed using the configurations shown in Fig. 1(c) and (d).

The distribution of the shear strain and strain energy density at a depth of 0.75 mm from the undeformed skin surface, derived from the 1PT and 2PT indentation models, is illustrated in Fig. 8(a) and (b), respectively. The shear strain profiles reverse direction at the contact points (due to the selection of the coordinate system), and the peak-to-peak variations in the strain around the contact point decrease dramatically when the indentor spacing decreases from 4.0 to 1.5 mm, as shown in Fig. 8(a). The values of the strain energy density reach their peak values under the contact points, and these peak values also decrease when the indentor spacing decreases from 4.0 to 1.5 mm.

4. Discussion and conclusion

Tactile sensation of the human fingertips has been widely used for the assessment of health and function in persons who have prolonged exposure to hand-transmitted vibration [23] and carpal tunnel syndrome [24]. Tactile performance is associated with activity of the nerve endings at the fingertips, and the sensitivity of the soft tissue within the fingertip to the nature of static and dynamic skin indentation. In the present study, an anatomically based FE model of the fingertip was developed to investigate the biomechanics of tactile sensation. The multi-layered fingertip model used in this analysis has the advantage over the "waterbed" and "continuum" fingertip models in that it can predict the surface deflection of the fingertip, the stress and strain distribution within the soft tissues, and, most importantly, the dynamic responses of the fingertip to mechanical stimuli. The present study represents the first theoretical analysis of the biomechanics of the tactile sensation in 1PT and 2PT discrimination tests.

The deflection profile of the skin surface subjected to a line load agrees well with experimental data and the results of the "waterbed" model [7] (Fig. 2(a)). Although the "waterbed" and our fingertip models give similar skin surface deflections under static loads, the proposed model differs considerably from the "waterbed" model when dynamic responses are considered.

The proposed model accounts for the effects of nonlinear and time-dependent mechanical properties of the skin and subcutaneous tissue, and, therefore, can be applied to study the dynamic behavior of the deflection profile of the skin surface (Fig. 2(b)). The "continuum" models reported by [9,10] predicted a dramatic increase in the skin surface deflection near the contact point, which was not consistent with their own experimental observations.

The calculated distributions of strain and strain energy density within the skin tissue (Fig. 5) showed reasonably good qualitative agreement with those predicted from the "continuum" model [10]. However, the peak strain and strain energy density values derived from the current model are approximately 50–80% greater than those predicted from the "continuum" model [10]. It is likely that the strain values predicted using our model are more realistic than those obtained using the "continuum" model, because our deflection profiles of the skin surface agree well with the reported experimental data [7] and the spatial displacement within the soft tissue is continuous. However, there are no appropriate experimental data on stress/strain fields within soft tissues for comparison with our predictions.

The model results for the 2PT discrimination tests reveal that differences in the normal strains (horizontal and vertical strains) and strain energy density developed in the skin at the contact points and at the geometric center of the fingertip vary little with a decrease in the indentor spacing from 4.0 to 3.0 mm (Fig. 9), but decreased considerably with a further decrease in the indentor spacing from 3.0 to 2.0 mm (Fig. 9). The corresponding differences in the vertical displacement and shear strain, however, decreased almost linearly with the decrease in the indentor spacing from 4.0 to 1.5 mm. Assuming that the mechanoreceptors in the dermis sense the stimuli associated with normal strains (the vertical and horizontal strains) and strain energy density rather than those associated with shear strain, the threshold of 2PT discrimination test for the fingertip may lie between 2.0 and 3.0 mm based on the present analysis, which is consistent with the experimental observations by Perez et al. [25] who reported an average 2PT discrimination distance of 2.1 mm in vibrotactile tests of the index finger.

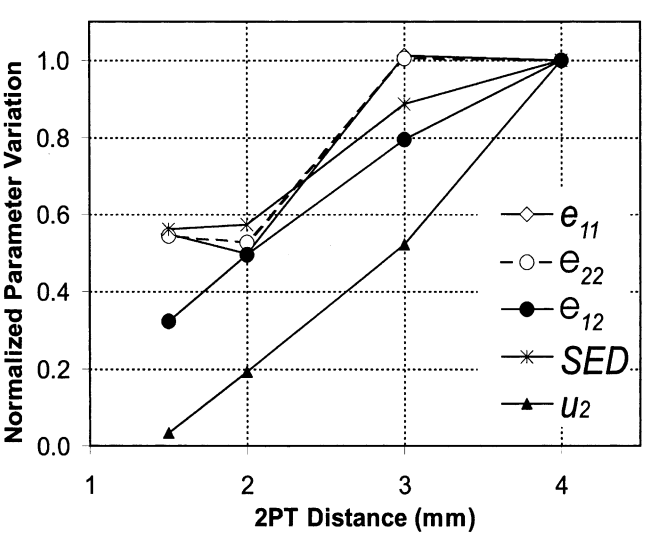

Fig. 9. Normalized variations of horizontal (e_{11}), vertical (e_{22}) and shear strains (e_{12}), vertical displacement (u_2), and strain energy density (SED) as a function of 2PT spacing. The normalized variations were evaluated by $[f_{(\text{contact point of indentor})} - f_{(\text{geometry center})}]/f_{(\text{contact point of indentor})}$ with $f = e_{11}, e_{22}, e_{12}, u_2$, and SED, as shown in Figs. 6–8.

As the distance from the indenting wedge exceeds 3.0 mm, the predicted profile of the skin surface deflection at the steady-state deviates from the measured data [7], as shown in Fig. 2. This deviation may be attributed to the differences between the configurations in the experimental measurement and the FE model. In the experiment [7], the profile of the skin deflection was measured along the longitudinal direction of the finger; while in the FE model, it is predicted to be perpendicular to the longitudinal direction of the finger. It is accepted that in the vicinity of the indenting wedge, boundary condition has less effect on the skin surface deflection, such that the results from 2D fingertip models [10] are comparable to the experimental results [7].

In the tactile sensation tests, such as the tests of 2PT discrimination and vibrotactile sensation threshold, the testing results may depend on many factors, such as the magnitude and the speed of the indentations, the conditions of the surrounding supports on the fingers, and the dimensions of the indenters. It is technically difficult to quantitatively evaluate how these factors influence the testing results through an experimental approach. The proposed theoretical model is capable of determining the time-dependent stress/strain distributions in a cross-section of the fingertip. The proposed approach can be applied to mimic the mechanical stimuli which the mechanoreceptors (i.e. Parisian and Meissner's corpuscles) in the fingertip sense during the tactile sensation tests. The potential impacts of the varied test conditions on the measurements can be analyzed quantitatively. Therefore, the proposed approach can be applied to help improve the reliability of the tactile sensation tests.

Appendix A. Constitutive equation for the skin

The skin is assumed to experience large deformation and possess nonlinearly elastic and linearly viscoelastic properties. The total tissue stress ($\tilde{\sigma}$) is assumed to be composed of elastic ($\tilde{\sigma}^0$) and viscous ($\tilde{\sigma}^{\mathrm{v}}$) stress components, such that [26]

$$\tilde{\sigma}(t) = \tilde{\sigma}^0(t) + \tilde{\sigma}^{\mathrm{v}}(t) = \tilde{\sigma}^0(t) + \int_0^t \frac{\dot{G}(\tau)}{G_0}\tilde{\sigma}^0(t-\tau)\mathrm{d}\tau = \tilde{\sigma}^0(t) + \int_0^t \dot{g}(\tau)\tilde{\sigma}^0(t-\tau)\mathrm{d}\tau \quad (1)$$

where t is time. Here the deformation behavior during the volumetric relaxation is considered to be identical to that attained under shear relaxation. The stress relaxation function is defined using the Prony series [27]

$$g(t) = \frac{G(t)}{G_0} = \left[1 - \sum_{i=1}^{N_G} g_i(1-\mathrm{e}^{-t/\tau_i})\right] \quad (2)$$

where G_0 and $G(t)$ are the instantaneous and time-dependent moduli, respectively; g_i and τ_i ($i = 1, 2, \ldots, N_G$) are stress relaxation parameters; N_G is the number of terms used in the stress relaxation function.

The elastic deformation behavior of the soft tissue, based on finite deformation theory, is assumed to be nonlinearly elastic (hyperelastic). A function of strain energy density per unit volume, U, defined for the elastometric foams [28] is applied to describe the elastic behavior of the tissue in the following manner:

$$U = \sum_{i=1}^{N} \frac{2\mu_i}{\alpha_i^2}\left[\lambda_1^{\alpha_i} + \lambda_2^{\alpha_i} + \lambda_3^{\alpha_i} - 3 + \frac{1}{\beta}(J^{-\alpha_i\beta} - 1)\right] \quad (3)$$

where $J = \lambda_1\lambda_2\lambda_3$ is the volume ratio, λ_i (i= 1, 2, 3) are the principal stretch ratios, α_i and μ_i ($i = 1, \ldots, N$) are the material parameters, $\beta = v/(1-2v)$ where v is the Poisson's ratio, and N is the number of terms used in the strain energy function.

The elastic stress $\tilde{\sigma}^0$ is related to the elastic strain energy function (3) by

$$\tilde{\sigma}_0 = \frac{2}{J}\tilde{F}\frac{\partial U}{\partial \tilde{C}}\tilde{F}^{\mathrm{T}} \quad (4)$$

where $\tilde{F}$ and $\tilde{C}$ are the deformation gradient and the right Cauchy-Green deformation tensors, respectively.

Constitutive equation for the subcutaneous tissue

The subcutaneous tissue is modeled as a sponge-like porous material fully saturated with fluid. The biphasic models for articular cartilage [16,29,30] are adopted in the present study to simulate the biomechanical behavior of the subcutaneous tissue. Since the subcutaneous tissue undergoes large deformation, the poroelastic constitutive relation is formulated based on the finite deformation theory with a deformation-dependent hydraulic permeability. The tissue stress, $\tilde{\sigma}^{\mathrm{t}}$, is composed of the stresses in the solid and fluid phase, $\tilde{\sigma}^{\mathrm{s}}$ and $\tilde{\sigma}^{\mathrm{f}}$, respectively:

$$\begin{aligned} &\tilde{\sigma}^{\mathrm{t}} = \tilde{\sigma}^{\mathrm{f}} + \tilde{\sigma}^{\mathrm{s}} \\ &\tilde{\sigma}^{\mathrm{f}} = -\Phi^{\mathrm{f}} p\mathrm{I}, \quad \tilde{\sigma}^{\mathrm{s}} = \sigma_{\mathrm{e}}^{\mathrm{s}} - \Phi^{\mathrm{s}} p\mathrm{I} \end{aligned} \quad (5)$$

where Φ^{s} and Φ^{f}, with $\Phi^{\mathrm{s}} + \Phi^{\mathrm{f}} = 1$, are the instantaneous volume fractions of the solid and fluid phases, respectively; p is the fluid pressure; the superscripts s and f imply the solid and fluid phase, respectively. The deformation-related stress in the solid phase, $\tilde{\sigma}_{\mathrm{e}}^{\mathrm{s}}$, is considered as nonlinearly elastic (hyperelastic) and is determined using Eqs. (3) and (4).

The equation of motion of the tissue is governed by:

$$\nabla \cdot \tilde{\sigma}^{\mathrm{s}} + \tilde{\pi}^{\mathrm{s}} = 0, \quad \nabla \cdot \tilde{\sigma}^{\mathrm{f}} + \tilde{\pi}^{\mathrm{f}} = 0 \quad (6)$$

where $\tilde{\pi}^{\mathrm{f}}$ and $\tilde{\pi}^{\mathrm{s}}$ are the momentum exchanges, given by:

$$\tilde{\pi}^{\mathrm{f}} = -\tilde{\pi}^{\mathrm{s}} = \Phi^{\mathrm{s}}\nabla p + K(\tilde{v}^{\mathrm{s}} - \tilde{v}^{\mathrm{f}}) \quad (7)$$

where $\tilde{v}^{\mathrm{f}}$ and $\tilde{v}^{\mathrm{s}}$ are the speed of the fluid and solid phases, respectively; K is the diffusive drag constant, which measures the frictional resistance of the fluid flowing through the solid matrix and is related to the hydraulic permeability, k, by $K = (\Phi^{\mathrm{f}})^2/k$.

The continuity condition of the tissue can be derived from the mass balance:

$$\nabla \cdot (\Phi^{\mathrm{s}}\tilde{v}^{\mathrm{s}} + \Phi^{\mathrm{f}}\tilde{v}^{\mathrm{f}}) = 0 \quad (8)$$

Owing to large deformations, the hydraulic permeability is considered to be deformation-dependent. The constitutive law of deformation-dependent permeability proposed by Holmes and Mow [30] is adopted, which is expressed in term of the void ratio [31], $e = \Phi^{\mathrm{f}}/\Phi^{\mathrm{s}}$, such that:

$$k = k_0\left(\frac{e}{e_0}\right)^{\kappa} \exp\left\{\frac{M}{2}\left[\left(\frac{1+e}{1+e_0}\right)^2 - 1\right]\right\} \quad (9)$$

where e_0 is the void ratio in the undeformed state; M and κ are the material parameters. For the undeformed state ($e = e_0$), Eq. (9) yields $k = k_0$; and under very large deformations ($e \to 0$), $k \to 0$.

Material parameters

The Young's moduli of the bone and nail were assumed, according to the published experimental data [32], to be 17.0 GPa and 170.0 MPa, respectively; while Poisson's ratio was assumed to be 0.30 for both. The material parameters of the skin and subcutaneous tissues used in the present simulations were determined based on the published experimental data [12,14,33,34], as in Table 1. The hydraulic permeability of the soft tissue has not been measured experimentally to date. It has been assumed that the permeability of the soft

Table 1
Material parameters of soft tissues

i	1	2	3
Material parameters characterizing hyperelasticity and viscoelasticity for the skin ($v = 0.40$)			
α_i	4.941	6.425	4.712
μ_i (MPa)	-7.594×10^{-2}	1.138×10^{-2}	6.572×10^{-2}
g_i	0.148	0.252	–
τ_i (s)	2.123	9.371	–
Material parameters characterizing the hyperelasticity for the subcutaneous tissue ($v = 0.40$)			
α_i	5.511	6.571	5.262
μ_i (MPa)	-4.895×10^{-2}	9.889×10^{-3}	3.964×10^{-2}
Material parameters of hydraulic permeability for the subcutaneous tissue			
M	κ	k_0 (m^4/Ns)	e_0
4.638	0.0848	1.0×10^{-15}	1.5

tissue is similar to that of articular cartilage [30], as suggested by Zhang et al. [15] (see Table 1).

References

[1] Guyton A. Human physiology and mechanisms of disease, 3rd ed.. Philadelphia: W.B. Saunders Co; 1982.

[2] Srinivasan M, LaMotte R. Tactile discrimination of shape: responses of slowly and rapidly adapting mechanoreceptive afferents to a step indented into the monkey fingerpad. J Neurosci 1987;7:1682–97.

[3] Verrillo RT, Gescheider GA. Effect of prior stimulation on vibrotactile thresholds. Sens Processes 1977;1:292–300.

[4] Gray H. Anatomy of the human body, 29th ed. Philadelphia: Lea and Febider; 1973.

[5] Vallbo AB, Johnson RS. Properties of cutaneous mechanoreceptors in the human hand related to touch sensation. Hum Neurobiol 1984;3:3–14.

[6] Fawcett D. Text book of histology, 11th ed.. Philadelphia: W.B. Saunders Co; 1986.

[7] Srinivasan M. Surface deflection of primate fingertip under line load. J Biomech 1989;22:343–9.

[8] Serina E, Mockensturm E, Mote CJ, Rempel D. A structural model of the forced compression of the fingertip pulp. J Biomech 1998;31:639–46.

[9] Phillips J, Johnson K. Tactile spatial resolution. iii: A continuum mechanics model of skin predicting mechanoreceptor responses to bars, edges, and gratings. J Neurophysiol 1981;46:1204–25.

[10] Srinivasan M, Dandekar K. An investigation of the mechanics of tactile sense using two-dimensional models of the primate fingertip. ASME J Biomech Eng 1996;118:48–55.

[11] Wu JZ, Dong RG, Smutz WP, Schopper AW. Modeling of time-dependent force response of fingertip to dynamic loading. J Biomech 2003;36:383–92.

[12] Zheng Y, Mak A. An ultrasound indentation system for biomechanical properties assessment of soft tissues in-vivo. IEEE Biomed Eng 1996;43:912–8.

[13] Rubin M, Bodner S, Binur N. An elastic–viscoplastic model for excised facial tissues. ASME J Biomech Eng 1998;120:686–9.

[14] Wan AW. Biaxial tension test of human skin in vivo. Biomed Mater Eng 1994;4:473–86.

[15] Zhang J, Mak A, Huang L. A large deformation biomechanical model for pressure ulcers. ASME J Biomech Eng 1997;119:406–8.

[16] Mow VC, Kuei SC, Lai WM, Armstrong CG. Biphasic creep and stress relaxation of articular cartilage: theory and experiment. ASME J Biomech Eng 1980;102:73–84.

[17] Harada N, Griffin M. Factors influencing vibration sense thresholds used to assess occupational exposures to hand transmitted vibration. Br J Ind Med 1991;48:185–92.

[18] Clemente CD. Anatomy: a regional atlas of the human body, 2nd ed. Baltimore, Munich: Urban and Achwarzengerg; 1981.

[19] Wu JZ, Dong RG, Schopper AW, Smutz WP. Analysis of skin deformation profiles during sinusoidal vibration of fingerpad. Ann Biomed Eng 2003;31(7):867–78.

[20] HKS. ABAQUS theory manual (version 5.8). Pawtucket (USA): Hibbitt, Karlsson and Sorensen, Inc.; 1998.

[21] Simon BR. Multiphasic poroelastic finite element models for soft tissue structures. Appl Mech Rev 1992;45:191–218.

[22] Wu JZ, Herzog W, Epstein M. Evaluation of the finite element software ABAQUS for biomechanical modelling of biphasic tissues. J Biomech 1998;31:165–9.

[23] ISO/FDIS-13091-1. International Standard: Mechanical Vibration—Vibrotactile perception thresholds for the assessment of nerve dysfunction—Part 1: Methods of measurement at the fingertips. The International Organization for Standardization, 2001.

[24] Morrissey S, Winn F, Bittner A. Screening for carpal tunnel syndrome with vibration threshold testing. Ergonomics Society of Taiwan, Technical Report, 1996.

[25] Perez C, Holzmann C, Jaeschke H. Two-point vibrotactile discrimination related to parameters of pulse burst stimulus. Med Biol Eng Comput 2000;38:74–9.

[26] Lockett FJ. Nonlinear viscoelastic solids. London, New York: Academic Press; 1972.

[27] Tschoegl NW. The phenomenological theory of linear viscoelastic behavior: an introduction. New York: Springer-Verlag; 1989.

[28] Storakers B. On material representation and constitutive branching in finite compressible elasticity. J Mech Phys Solid 1986;34:125–45.

[29] Holmes M. Finite deformation of soft tissue: analysis of a mixture model in uni-axial compression. ASME J Biomech Eng 1986;108:372–81.

[30] Holmes M, Mow VC. Nonlinear characteristics of soft gels and hydrated connective tissues in ultrafiltration. J Biomech 1990;23:1145–56.

[31] Wu JZ, Herzog W. Finite element simulation of location- and time-dependent mechanical behavior of chondrocytes in unconfined compression tests. Ann Biomed Eng 2000;28:318–30.

[32] Yamada H. Strength of biological materials. Baltimore: Williams and Wilkins Co; 1970.
[33] Pan L, Zan L, Foster F. Ultrasonic and viscoelastic properties of skin under transverse mechanical stress in vitro. Ultrasound Med Biol 1998;24:995–1007.
[34] Miller-Young J, Duncan N, Baroud G. Material properties of the human calcaneal fat pad in compression: experiment and theory. J Biomech 2002;35:1523–32.